Inorganic Chemistry

pubs.acs.org/IC Article

Enlarging Quantum Coherence of Vanadyl Spin Qubits in Zirconium Porphyrinic MOFs

Lucija Vujević, Gregor Talajić, Fraser MacMillan, Alexey A. Popov, Marina Kveder, Bahar Karadeniz,* Krunoslav Užarević,* and Dijana Žilić*

Cite This: Inorg. Chem. 2026, 65, 7603−7612

Read Online

ACCESS | Metrics & More | Article Recommendations | Supporting Information

ABSTRACT: The intrinsic quantum−mechanical properties of electron spin along with the structural and chemical tunability of metal−organic frameworks (MOFs) that can control the position of the active spin carrier make molecular spin qubits embedded in porous coordination frameworks an ideal platform for investigating quantum coherence. These molecular spin qubits still exhibit relatively short relaxation times, but several recently developed strategies hold promise for extending coherence. We recently demonstrated that diluting the copper(II)-porphyrin qubits, combined with the inclusion of fullerene C_{60} guests, can significantly prolong the relaxation times to liquid nitrogen temperature. Here, we present how the exchange of copper(II)-with the vanadyl-porphyrin spin qubits allows for a more diluted qubit framework and results in a stable system with one of the longest coherence times observed in the nonactivated MOF qubit frameworks. The fullerene inclusion proved beneficial for both the electron spin−lattice and the phase-memory times. Figures of merit T_m ~1 μs were observed in the temperature range 5−180 K, while the coherence was detected up to 240 K and still was not T_1-limited. The detected linear dependence of the Rabi frequency on the microwave field confirmed that the tested vanadyl frameworks are viable qubit candidates.

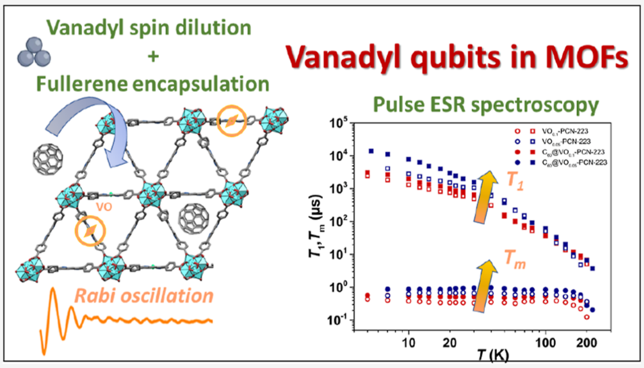

■ INTRODUCTION

The search for viable quantum bits or qubits, the basic units of quantum computers, is one of the main goals in materials science today. Different physical realizations of qubit candidates, such as the polarization state of a photon, trapped atoms, superconducting circuits, quantum dots, Bose−Einstein condensates, nuclear spins, and electron spins, have distinct merits and drawbacks.[1−9] Molecular complexes that exploit electron spin can yield highly reproducible qubits, which can be designed using coordination-chemistry tools and chemical modifications.[1,3] However, one of the main disadvantages of molecular spin qubits is relatively short relaxation times compared to other qubit candidates.[10] The lifetime of qubit superposition is determined by the spin−spin relaxation time T_2, experimentally measured as a phase-memory time T_m. For transition metal ions at higher temperatures (liquid nitrogen regime), the T_m time is limited by the spin−lattice relaxation time T_1.[1,3] In recent decades, intensive research has been conducted to improve coherence and understand which factors influence the relaxation processes in molecular-based qubits, and the standard strategies include the careful choice of transition metal or rare-earth ions, ligands, solvents, and qubit spatial division in the long-order structure.[4,11−18]

Metal−organic frameworks (MOFs)[19−21] are a particularly interesting class of materials for qubit stabilization because of their modularity, stability, and tunable porous structures, where qubits can be controllably separated in three dimensions in the framework based on ligand geometry and metal-node coordination preferences. Among these, zirconium-porphyrinic MOFs have already been proven as an excellent platform for the formation of three-dimensional spin-qubit frameworks. Zirconium(IV)−carboxylate bonds provide unprecedented stability in various conditions, regardless of large pores, while porphyrin spacers isolate and separate coordinated paramagnetic centers within well-defined frameworks.[22] Freedman and co-workers first demonstrated cobalt(II)-tetrakis(4-carboxyphenyl)porphyrin (cobalt(II)-TCPP) qubits in the PCN-224 framework, achieving T_m ~2 μs up to 15 K.[23] Subsequently, the same group reported how copper(II)-TCPP qubits in PCN-224 exhibit a detectable coherence of 0.16 μs

Received: October 17, 2025
Revised: March 10, 2026
Accepted: March 20, 2026
Published: March 30, 2026

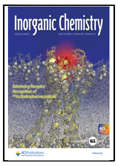

up to 80 K.[24] However, although PCN-224 provides an important platform for these advances, its low connectivity to the zirconia cluster (6-connected) and very large pores may reflect in lower chemical and thermodynamic stability.[25−27]

Our group has reported a method to improve the performance of molecular spin qubits in a robust and moderately porous, twelve-coordinated PCN-223[25,28] matrix by mechanochemical qubit dilution and inclusion of fullerene guests in the MOF voids.[29] The C_{60} fullerenes acted as a template, directing the mechanochemical formation exclusively to the hexagonal PCN-223 fulleretic composites. They reside in the trigonal channels of the PCN-223 (Figure 1), near the porphyrin core.[29] The introduction of fullerenes extends the coherence time T_m by removing the nuclear spin-bearing solvent from the pores and influencing the spin−lattice time T_1. In the maximum, 10% dilution of copper(II) porphyrin qubits (Cu-TCPP), the best performing fulleretic PCN-223 composite showed a phase-memory coherence of $T_m = 0.8\ \mu s$ at 5 K and detectable coherence of $T_m = 0.2\ \mu s$ up to 80 K. While this strategy is shown to strongly affect coherence among the copper-TCPP molecular qubits in the framework, achieving longer coherence times at higher temperature, and a comprehensive understanding of the nature of vibrations and spin−phonon coupling in framework qubit materials remains a challenging task.[30]

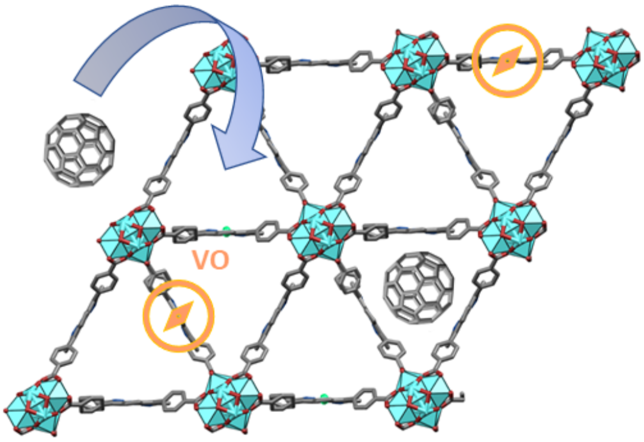

Figure 1. Twelve-coordinated hexagonal Zr-PCN-223 framework with 10% or 5% spin-active VO-TCPP building the framework and fullerene within the channels of the formed MOF.

Here, we present a series of spin-active PCN-223 MOFs and composites achieved by exchanging the copper-TCPP qubits with oxovanadium(IV)-TCPP, allowing a direct comparison of their performance and yielding key insights into the role of metal centers in determining qubit performance.[31] The vanadyl ion (oxovanadium(IV), VO^{2+}) is known for its stable and high coherence in the liquid nitrogen regime and it can be incorporated into a wide range of molecular scaffolds,[10,16,23,30−38] which allows fine-tuning of their magnetic and electronic properties.[39] We study the effects of both pore content modification and high-spin dilution on the electron spin dynamics of targeted qubit frameworks. The exchange of copper with vanadyl enabled high-spin dilution to 5% vanadyl-TCPPs, which construct the Zr-MOF framework with a diamagnetic zinc−TCPP diluent. The incorporation of fullerene into the MOF pores was examined as a strategy to further extend the relaxation times. The resulting fulleretic composite materials were characterized by powder X-ray diffraction (PXRD) and Fourier-transform infrared (FTIR) spectroscopy to clarify their structures and connectivity. Electron spin resonance (ESR) has proven to be an ideal experimental technique for characterizing, manipulating, and controlling electron spin qubits. Continuous-wave (CW) ESR spectroscopy was used to gain insight into the local magnetic properties of the vanadium(IV) center described by the spin-Hamiltonian parameters. Hyperfine sublevel correlation spectroscopy (HYSCORE) was performed to probe the weaker superhyperfine interactions between the electron spin and nearby nuclei from the porphyrin ring. Pulsed ESR was used to obtain electron spin−lattice (T_1) and phase-memory (T_m) relaxation times. Nutation experiments and the detection of Rabi oscillation tested the potential of these framework qubits for quantum information processing. Investigated vanadyl-zinc PCN-223 MOFs and their fulleretic composites were compared for their qubit performance to copper(II) analogs,[29] as well as to other similar VO spin qubits.[10,16,32]

■ EXPERIMENTAL SECTION

Synthesis: All solvents and reagents obtained from commercial sources were used without further purification. Pyrrole, methyl 4-formylbenzoate, *p*-nitrobenzaldehyde, propionic acid, pyridine, and acetic anhydride were purchased from Merck. Methanol (MeOH), chloroform (CH_3Cl), and dimethylformamide (DMF) were purchased from Lachner. Zinc chloride, vanadyl acetylacetonate (VO-$(acac)_2$), diethylformamide (DEF), and sodium acetate (NaOAc) were supplied from Sigma-Aldrich. Zr_{12}-acetate $(Zr_6O_4(OH)_4(CH_3COO)_{12})_2)$ and Zr_6-methacrylate $(Zr_6O_4(OH)_4(C_2H_3COO)_{12})$ clusters were synthesized according to the literature methods.[40,41] 5,10,15,20-Tetrakis(4-methoxycarbonylphenyl)porphyrin (TPPCOOMe) was prepared according to the literature.[42] FTIR and PXRD data were in accordance with previously published data for these compounds. Vanadyl-tetra(4-carboxyphenyl)porphine (VO-TCPP) was synthesized according to the literature methods.[10]

The $C_{60}@(VO)_{0.1}$-PCN-223 Zr_6-methacrylate cluster (20.2 mg, 0.012 mmol), VOTCPP (2.43 mg, 0.0026 mmol), ZnTCPP (20 mg, 0.0236 mmol), NaOAc (7.5 mg), C_{60} (18 mg, excess), and DMF (45 μL) were placed into a Teflon jar (14 mL) with two zirconia balls (1.6 g each). The reaction mixture was milled using an IST-500 (InSolido Technologies, Croatia) mixer mill at 30 Hz for 90 min. The resulting black powder was washed with toluene (5 × 5 mL) and DMF (3 × 4 mL).

$C_{60}@(VO)_{0.05}$-PCN-223 was prepared similarly to that described for $C_{60}@(VO)_{0.1}$-PCN-223 by reacting 1.136 mg of VOTCPP (0.0012 mmol). The resulting black powder was washed with toluene (5 × 5 mL) and DMF (3 × 4 mL).

The $(VO)_{0.1}$-PCN-223 Zr_{12}-acetate cluster (19.95 mg, 0.006 mmol), VOTCPP (2.43 mg, 0.0026 mmol), ZnTCPP (20 mg, 0.0234 mmol), NaOAc (6 mg), and DEF (30 μL) were placed into a Teflon jar (14 mL) with two zirconia balls (1.6 g each). The reaction mixture was milled using an IST-500 (InSolido Technologies, Croatia) mixer mill at 30 Hz for 90 min. The resulting dark purple powder was washed with DMF (3 × 4 mL).

$(VO)_{0.05}$-PCN-223 was prepared similarly to that described for $C_{60}@(VO)_{0.1}$-PCN-223 by reacting 1.136 mg of VOTCPP (0.0012 mmol). The resulting dark purple powder was washed with DMF (3 × 4 mL).

PXRD: Powder X-ray diffraction measurements were performed on a Panalytical Aeris Research tabletop diffractometer equipped with Cu Kα radiation (40 kV, 7.5 mA) in Bragg−Brentano geometry.

FTIR-ATR: Fourier-transform infrared attenuated total reflectance spectra were recorded on a PerkinElmer Spectrum Two spectrometer equipped with a diamond ATR cell. Data were collected over the

4400−400 cm^{-1} range with a resolution of 4 cm^{-1} and processed using Spectrum software (version 10.5.3.738, 2016).

CW ESR: Continuous-wave ESR experiments were performed using an X-band FT/CW Bruker ELEXSYS 580 spectrometer with an Oxford Instruments temperature unit. Experiments were carried out with a modulation amplitude of 0.1 mT at 100 kHz modulation frequency using a microwave power of 0.2012 mW.

Magnetization decay rates were recorded in the temperature range 5−220 K using a $\pi/2$ pulse of 16 ns. Two-pulse echo-detected field-swept ESR spectra were recorded at T = 80 K using the pulse sequence $\pi/2-\tau-\pi-\tau$−echo, with τ = 200 ns to select a spectral position for the relaxation-time experiments.

HYSCORE experiments were performed using the sequence $\pi/2-\tau-\pi/2-t_1-\pi-t_2-\pi/2-\tau$−echo, τ = 100 ns. The time intervals t_1 and t_2 with starting values of 200 ns were varied in 150 steps of 16 ns.[43]

Spin−lattice relaxation times, T_1, were recorded using an inversion recovery (IR) pulse sequence with an echo detection sequence, $\pi-t-\pi/2-\tau-\pi$−echo, where τ = 200 ns and variable t starts from the initial value of 400 ns.[43] T_1 relaxation time was determined from a fit of the echo recovery amplitude to the biexponential function:

$$I = I_0 + k_1 e^{-\tau/T_{1a}} + k_2 e^{-\tau/T_{1b}} \quad (1)$$

wherein the longer component $T_{1a} > T_{1b}$ was taken as an approximation of T_1.[44]

To get a better agreement of fit for spin−lattice relaxation rate given by eq 2 with experimental data, the fit included weights of experimental points calculated as inverse values of squared experimental errors, $(1/Err^2)$.[45]

Saturation recovery experiments were performed using a picket-fence sequence of eight microwave pulses of 16 ns, followed with a two-pulse echo sequence $\pi/2-\tau-\pi-\tau$−echo with π = 32 ns and τ = 200 ns.

The phase-memory time, T_m, was obtained using a two-pulse electron-spin−echo decay sequence, $\pi/2-\tau-\pi-\tau$−echo, with τ = 200 ns and shots repetition time was adjusted to accommodate complete spin−lattice relaxation. T_m was determined by fitting the echo signal to the monoexponential decay function:[43]

$$I = I_0 + k_m e^{-\tau/T_m} \quad (2)$$

Measurements of echo-detected Rabi oscillations were obtained with the following pulse sequence $t_p-T-\pi/2-\tau-\pi-\tau$−echo. Here, the nutation pulse length t_p was varied and τ = 200 ns and T = 1000 ns. The time duration of the nutation pulse, t_p, was increased from 12 to 32 ns and was adjusted by choosing the proper microwave power attenuation (0 dB−11 dB) to achieve maximal spin−echo signal ($\beta = \pi/2$)[43] while the field strength was calculated from δt and β.[46,47]

■ RESULTS AND DISCUSSION

Synthesis and Structural Characterization

$(VO)_n$-PCN-223 MOFs and $C_{60}@(VO)_x$-PCN-223 (x: 0.05 and 0.1) composites were synthesized mechanochemically in accordance with our previously reported procedures,[28,29] with detailed experimental information provided in the Supporting Information, Section 1.1.

The crystallinity and phase purity of the spin-diluted PCN-223 derivatives, with 10% and 5% VO-TCPP, with and without fullerene incorporation, were first examined by PXRD. The diffraction patterns of all samples (Figure 2) matched well with the simulated pattern of PCN-223 (Cambridge Crystallographic Data Centre (CCDC) code: TUTWUC) after the mechanochemical vanadyl dilution and fullerene loading. Significant changes in low-angle peak (4.8 Å) intensities were observed upon fullerene incorporation, which can be attributed to changes in the electron density of the pore content.[29,48] FTIR spectroscopy data shown in Figure S1 are consistent with those reported for the PCN-223 compounds and fulleretic composites.[28,29,48]

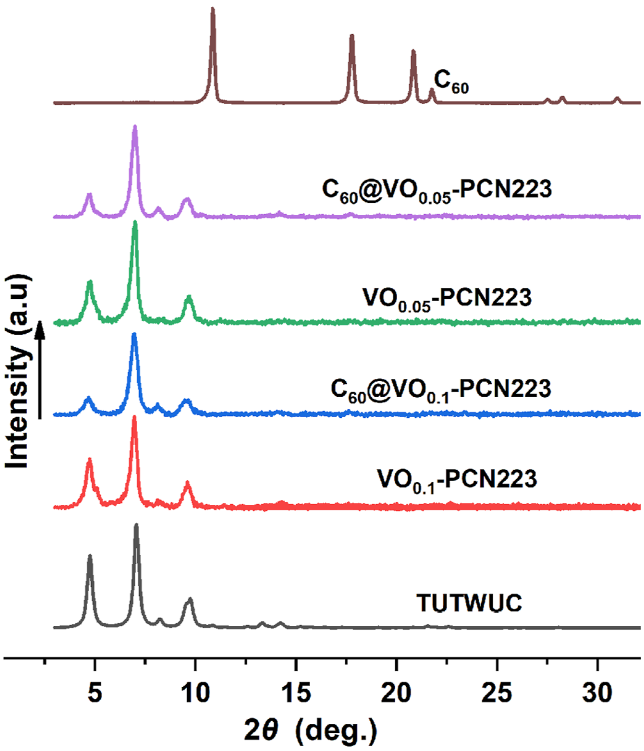

Figure 2. PXRD data for prepared $(VO)_x$-PCN-223 MOFs and the $C_{60}@(VO)_x$-PCN-223 (x: 0.05 and 0.1) composites vs simulated pattern for PCN-223 (CCDC: TUTWUC).

CW ESR Experiments

The CW ESR lines of VO ions are more pronounced in $(VO)_{1.0}$-PCN-223 than in VO-TCPP (Figures S2−S4) due to more separate spins and reduced spin−spin interactions. However, the quantum coherence of these samples, which contained only vanadyl ions in TCPP, was too short to be detected by pulse ESR. Experimental and simulated CW ESR spectra of MOFs with diluted spins, 10% VO and 5% VO, recorded at 80 K are shown in Figure 3 (left side). It can be noticed that both samples, $(VO)_{0.1}$-PCN-223 and $(VO)_{0.05}$-PCN-223, show a similar spectrum with 8 major lines as a consequence of the strong hyperfine coupling of the unpaired electron spin $S = 1/2$ with the vanadium ^{51}V nuclear magnetic spin $I = 7/2$ (natural abundance 99.75%).[49] The experimental spectra were simulated using EasySpin software,[50] assuming axial symmetry of the g tensor and A hyperfine tensor. Therefore, the following spin-Hamiltonian for vanadyl electron spin was used:

$$H = \mu_B BgS + SAI \quad (3)$$

where B is the external magnetic field while the constant μ_B is Bohr magneton. The parameters obtained from the simulations are given in Table 1 and are consistent with the data reported in the literature.[10,31] From Table 1, it can be noticed that the width of the Lorentzian line used for the simulation decreases as the VO concentration decreases, as expected due to reduced spin−spin interactions.

The CW ESR spectra of MOFs with incorporated fullerene $C_{60}@(VO)_{0.1}$-PCN-223 and $C_{60}@(VO)_{0.05}$-PCN-223 are presented also in Figure 3 (right side). Off-the-shelf fullerene

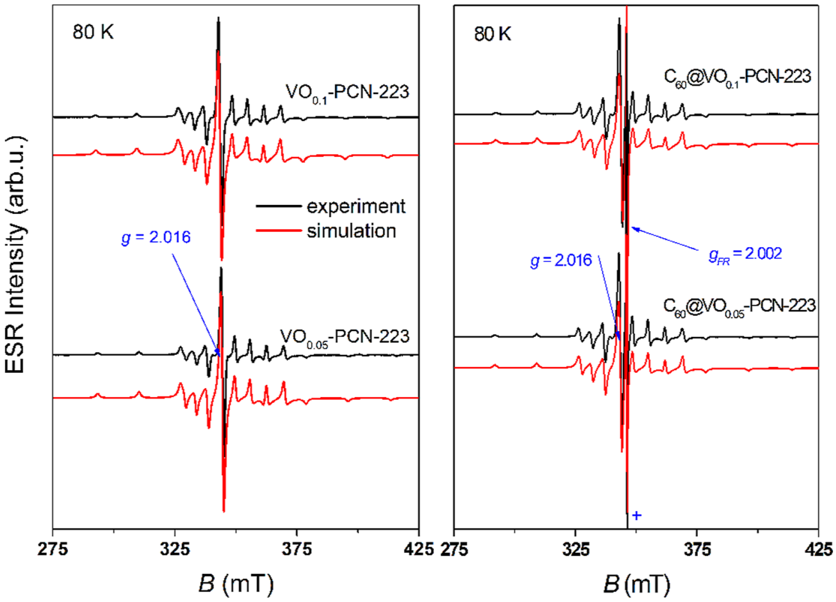

Figure 3. Experimental and simulated CW ESR spectra of MOFs with 10% and 5% VO at 80 K. Parameters used for the simulation are given in Table 1. Symbol "+" denotes truncation of the fullerene radicals (FR) peak with $g_{\mathrm{FR}} \approx 2.002$. $g = 2.016$ labeled the spectral position at which pulse experiments were performed.

Table 1. Spin Hamiltonian Parameters Derived according to Eq 1 Using the EasySpin Software Package[50] for the Simulation of CW ESR Spectra of the Investigated Samples at 80 K

compound	$(VO)_{0.1}$-PCN-223	$C_{60}@(VO)_{0.1}$-PCN-223	$(VO)_{0.05}$-PCN-223	$C_{60}@(VO)_{0.05}$PCN-223
$g_\parallel$	1.9652	1.9620	1.9645	1.9620
$g_\perp$	1.9827	1.9830	1.9827	1.9835
$A_\parallel^V$, MHz	469.6	478.0	471.5	479.0
$A_\perp^V$, MHz	158.0	163.0	161.0	165.0
Γ_L[a], mT	1.2	1.2	1.0	1.0
g_{FR}	-	2.00236	-	2.00236
W[a], mT	-	0.3	-	0.3

[a] Lorentzian line width of the CW ESR spectra.

shows ESR signal at $g_{FR} \approx 2.002$ due to defects, fullerene radicals (FR) in the structure.[48,51,52] Because of the presence of these fullerene radicals, the simulation of the experimental spectra was done in terms of a mixture of spin species by combining the spin-Hamiltonian of vanadyl given by eq 1 and the spin-Hamiltonian of FR while assuming $S_{\mathrm{FR}} = 1/2$: $H_{\mathrm{FR}} = \mu_{\mathrm{B}} B g_{\mathrm{FR}} S_{\mathrm{FR}}$, with the intensity ratio ≈50:1. Superhyperfine lines due to the interaction of vanadyl electron spin with four nitrogen nuclear spins from the porphyrin core are not resolved, as observed earlier for vanadyl porphyrins,[10,53−56] contrary to the well-resolved lines for the copper(II) qubits.[29] The origin of this difference lies in different orbitals occupied by unpaired electrons; vanadyl unpaired spin is in nonbonding ionic d_{xy} orbitals, while copper spin is in the $d_{x^2-y^2}$ orbital, causing significantly different ligand−metal covalency.[31]

Pulse ESR Experiments

Two-pulse echo-detected field-swept (EDFS) ESR spectra of the samples with and without encapsulated fullerene are almost identical, as can be seen in Figure 4. The fullerene radical (FR) line can be detected only at low temperatures. Namely, EDFS intensity is proportional to the number of spins and it is very weak due to FR low concentration.[51] From double integration of CW ESR spectra, it can be concluded that the number of FR is around 200 times lower than that of VO spins in

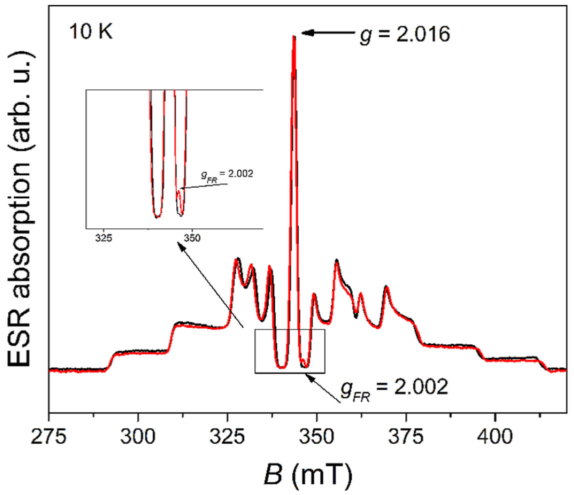

Figure 4. Two-pulse echo detected field-swept ESR spectrum of $(VO)_{0.05}$-PCN-223 (black line) and $C_{60}@(VO)_{0.05}$-PCN-223 (red line) recorded at $T = 10$ K. The relaxation measurements, as well as HYSCORE, were performed at the central line with $g = 2.016$, which corresponds to the $|M_S, I_S\rangle$ transition $\left|-\frac{1}{2}, -\frac{1}{2}\right\rangle \rightarrow \left|+\frac{1}{2}, -\frac{1}{2}\right\rangle$.[32,57] The line of fullerene radicals (FR), shown enlarged in the inset, has very low intensity due to their low concentration.

C_{60}@$(VO)_{0.05}$-PCN-223 sample. The relaxation time experiments for all MOF samples as well as HYSCORE were performed at the magnetic field of the central VO line with g = 2.016. This "powder-like position" corresponds to the $|M_S, I_S\rangle$ transition $\left|-\frac{1}{2}, -\frac{1}{2}\right\rangle \rightarrow \left|+\frac{1}{2}, -\frac{1}{2}\right\rangle$, where all molecules are excited due to the negligible angular dependency of the magnetic field.[32,57]

■ HYSCORE

HYSCORE experiments provide detailed information on the hyperfine interactions between the vanadyl unpaired electron and nearby nuclei in the porphyrin core and possible in solvent molecules. Namely, strong hyperfine coupling between the unpaired electron spin and ^{51}V nuclear spin with values $A_{\parallel}$ ≈470 MHz and $A_{\perp}$ ≈160 MHz (Table 1) obtained from CW ESR experiments is not detectable in HYSCORE experiments. HYSCORE shows weaker interactions, i.e., superhyperfine interactions between the electron and the nuclei such as ^{14}N, ^{13}C, and ^{1}H. The HYSCORE spectrum for the $(VO)_{0.05}$-PCN-223 sample is given in Figure 5a. The obtained spectrum is typical for vanadyl porphyrins.[10] The spectrum shows cross peaks, the correlations between nuclear transitions, in both (+,+) and (−,+) quadrants due to the superhyperfine interactions, and also the nuclear quadrupole interaction of the ^{14}N nuclei. All cross peaks related to stronger coupling with ^{14}N are shown in the (−,+) quadrant.[58] The most prominent cross peaks "1" and "2" are correlated to double-quantum (dq, $\Delta M_I = 2$) and single-quantum (sq, $\Delta M_I = 1$) ^{14}N transitions, respectively. The modulations "3" and "4", which relate to the weaker superhyperfine couplings with porphyrin ^{13}C and ^{1}H nuclei, respectively, are located close to their Larmor frequencies and are shown in the (+,+) quadrant.[10,58] The simulated HYSCORE spectrum with the spin-Hamiltonian parameters used for the simulation is given in Figure 5b. The obtained hyperfine and nuclear quadrupole splitting parameters for ^{14}N are in agreement with previously reported values for similar vanadyl porphyrin and phthalocyanine systems.[10] For ^{13}C and ^{1}H nuclei, their Larmor frequencies, 3.7 and 14.7 MHz, were used, respectively, while their quadrupole moments are zero. The fact that we obtained very similar HYSCORE spectra of all samples, independent of VO concentration (5% or 10%) and the presence or absence of fullerene in MOFs, Figures S5−S7 in the Supporting Information, and similar to others reported for VO-porphyrins,[10,58] confirms that HYSCORE shows superhyperfine interactions between unpaired electron and nuclei from the porphyrin core.

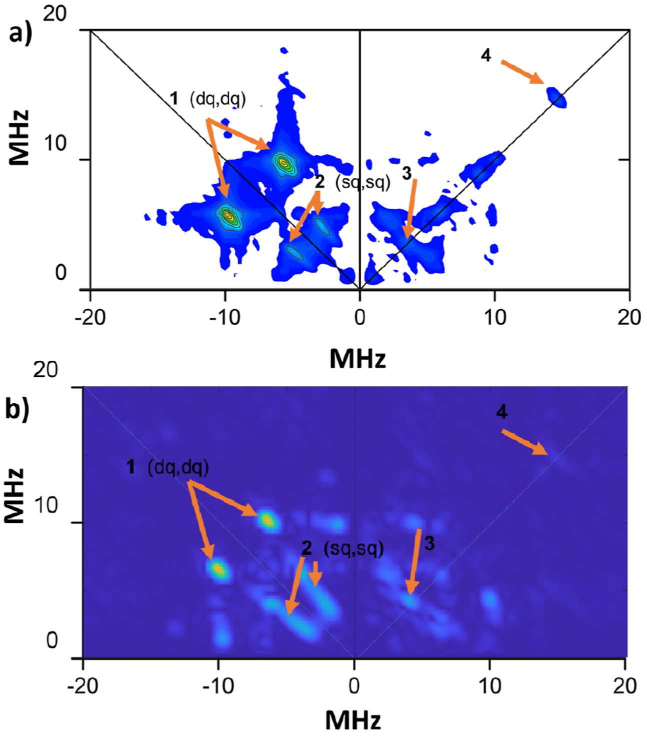

Figure 5. (a) HYSCORE spectrum recorded at 10 K at the g = 2.016 position (the highest peak) for the sample $(VO)_{0.05}$-PCN-223. (b) The simulated HYSCORE spectrum obtained using EasySpin[50] function saffron and sequence HYSCORE for interacting electron spin $S = 1/2$ with the following nuclei: ^{13}C nucleus with A = [0 3.7] MHz, Q = 0; ^{1}H nucleus with A = [0 14.7] MHz, Q = 0 and ^{14}N nucleus with A = [−6.8−6.8−7.8] MHz and Q = [5 0] MHz. Here, A and Q denote the hyperfine and nuclear quadrupole coupling tensors, respectively. The magnetic field value was used from the experiment 345.7 mT and τ = 100 ns.

Spin−Lattice Relaxation Time, T_1

The temperature dependence of the electron spin−lattice relaxation rate, $1/T_1$, for four investigated PCN-223 samples with 10% and 5% VO ions, with and without incorporated fullerene in MOF-channels, is shown in Figure 6 and Table S1.

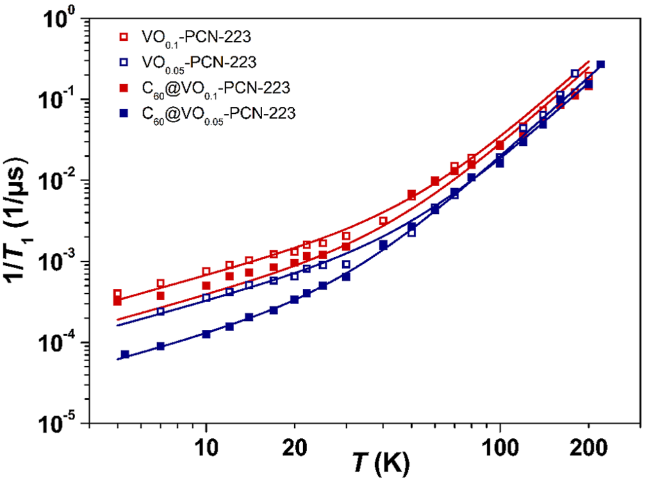

Figure 6. Temperature dependence of the electron spin−lattice relaxation rate $1/T_1$ of various MOFs. Full lines are best-fits of eq 4 to experimental data (squares) with the fitting parameters given in Table 2.

The spin echo was detected from the lowest experimental temperature, 5 K, up to 240 K. It can be seen that T_1 time increases as the VO concentration decreases from 10% to 5%, as was expected due to reduced spin−spin interactions. The same effect as for copper qubits[29] was observed here for vanadyl qubits—encapsulating fullerenes leads to prolongation of the T_1 relaxation time. For example, the value T_1 ≈11 ms was observed for C_{60}@$(VO)_{0.05}$-PCN-223 at 7 K, which is almost triple the value for the same sample but without fullerene in the pores, $(VO)_{0.05}$-PCN-223, T_1 ≈4 ms. The longest T_1 = 14 ms value detected for C_{60}@$(VO)_{0.05}$-PCN-223 at 5.3 K is the same as the value detected at 4.3 K for crystalline dispersion of VOPc in TiOPc in a stoichiometric ratio 1:1000.[16] It is the same order of magnitude as T_1

Table 2. Best-Fit Parameters Obtained by Fitting Eq 4 to the Experimental Spin−Lattice Relaxation Rate Data for Different MOF Samples

compound	$(VO)_{0.1}$-PCN-223	$C_{60}@(VO)_{0.1}$-PCN-223	$(VO)_{0.05}$-PCN-223	$C_{60}@(VO)_{0.05}$-PCN-223
a, $1/(K\mu s)$	$(6.6 \pm 0.4)\ 10^{-5}$	$(3.8 \pm 0.6)\ 10^{-5}$	$(3.2 \pm 0.1)\ 10^{-5}$	$(1.22 \pm 0.03)\ 10^{-5}$
b, $1/(K^n\mu s)$	$(7 \pm 5)\cdot 10^{-9}$	$(7 \pm 5)\ 10^{-9}$	$(4 \pm 1)\ 10^{-9}$	$(5 \pm 2)\cdot 10^{-9}$
n, −	3.3 ± 0.2	3.3 ± 0.3	3.30[a]	3.3 ± 0.1

[a] Fixed value used for fitting.

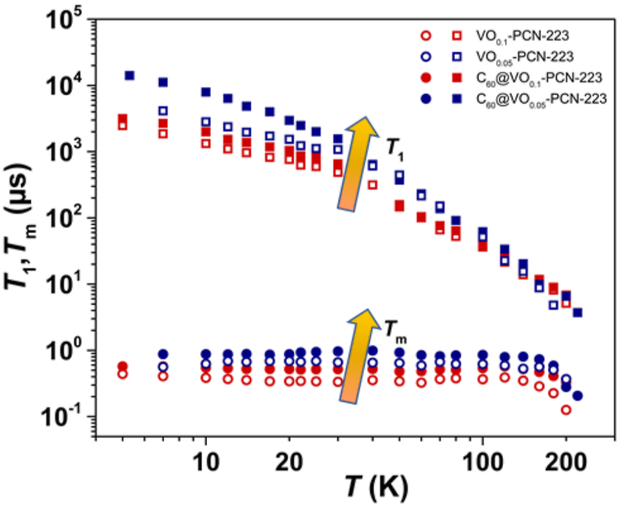

Figure 7. Comparison of the temperature dependence of the electron-spin phase-memory relaxation time, T_m, and spin−lattice relaxation time T_1 in all investigated PCN-223 with VO, presented in a log−log graph.

detected for 5% VO crystalline dispersion $[(Ph)_4P]_2[(VO)_{0.05}MoO_{0.95}(dmit)_2]$ (dmit = 1,3-dithiole-2-thione-4,5-dithiolate) and the deuterated version of the compound reported by the same group.[32] The most similar VO qubits 5% diluted in MOF $(VO)_{0.05}TiO_{0.95}$(TCPP-Zn_2-bpy) has T_1 ≈0.4 ms at 5 K.[10]

To better understand the spin−lattice relaxation and the influence of fullerene encapsulation, the underlying spin−phonon coupling mechanisms must be considered. As the choice of the pulse sequence, due to spectral diffusion effects at high spin concentrations, can affect T_1 values, we also performed saturation recovery experiments at a few selected temperatures.[59−62] The saturation recovery measurements were performed using an eight-picket-fence sequence for a more concentrated $C_{60}@(VO)_{0.1}$-PCN-223 sample.[24,63] From the obtained values given in Table S2, one can see a weak effect of spectral diffusion, and therefore, T_1 values obtained from inversion recovery experiments can be approximated as real values. The experimental data of the spin−lattice relaxation rate, $1/T_1$, were fitted using the known phenomenological expression for vanadyl qubits:[10,16,32,36,64]

$$1/T_1 = aT + bT^n \tag{4}$$

where the first term denotes a direct one-phonon process while the second term represents a two-phonon Raman process. The best-fit parameters are listed in Table 2.

The obtained values of parameters a and b, as well as parameter n ≈3, are in agreement with the values obtained for vanadyl qubits.[10,16,64,65] For the sample $(VO)_{0.05}$-PCN-223, a fixed value of $n = 3.3$ was taken to obtain reasonable fits. The lower values of parameter a observed upon fullerene encapsulation could indicate a slowing of the direct process. On the other hand, fullerene encapsulation does not significantly affect the parameter b or the Raman process. Therefore, from these experiments, we can conclude that fullerene encapsulation increases the spin−lattice relaxation time by slowing down the direct process. This is also in agreement with the fact that the T_1-increase upon fullerene encapsulating is the most pronounced at low temperatures, where the direct relaxation process is dominant.

Phase-Memory Relaxation Time, T_m

For vanadyl qubits reported in the literature, the thermal variation of the "observed" or "effective" spin−spin relaxation time, T_2, called the phase-memory time, T_m, shows an almost temperature-independent behavior below ∼100 K.[10,16,31] A similar behavior was observed for the investigated qubits, on the lin−lin scale in Figure S8 and Table S1 in the Supporting Information and in the log−log scale in Figure 7. As expected, phase-memory time increases with spin dilution due to reduced spin−spin interaction. For the best performing framework, $C_{60}@(VO)_{0.05}$-PCN-223, the phase-memory time has a nearly constant value of T_m ≈1 μs over 5−180 K, then decreases to 0.2 μs at 220 K and further 0.07 μs at 240 K. The similar 5% VO qubits, diluted in MOF $(VO)_{0.05}TiO_{0.95}$(TCPP-Zn_2-bpy), showed a T_m time of around 0.5 μs in the 5−100 K range.[10] For comparison, other vanadyl qubit materials, such as for the molecular dispersion of VOPc in TiOPc at a stoichiometric ratio of 1:1000, demonstrate a value of 2.04−3.41 μs observed in a similar temperature range (4.3−150 K).[16] The values of T_m from 1.6 to 8.7 μs in the range 4.5−100 K are detected for 5% VO crystalline dispersion $[(Ph)_4P]_2[(VO)_{0.05}MoO_{0.95}(dmit)_2]$ and the deuterated compound.[32] The results show that encapsulation of fullerenes in the $(VO)_{0.1}$-PCN-223 matrix enlarges T_m relaxation time due to partial replacement of the nuclear spin-active solvent (DMF) in pores with almost nuclear-spin-free fullerene molecules, containing only ^{13}C isotopes with around 1% having nuclear spin $I = 1/2$. The same effect was observed earlier for encapsulating fullerene in PCN-223 with embedded copper qubits.[29] After fullerene inclusion, the upper limit at which the coherence of the vanadyl qubit is experimentally detected increases from 200 to 240 K.

Rabi Oscillations

To prove that the detected coherence times allow coherent manipulation between the spin states,[23,57,66] the nutation experiments at different microwave powers were performed. Rabi oscillations were clearly observed at a liquid nitrogen temperature of 78 K, as shown in Figure 8a. The Rabi frequency ν_R, which describes the interaction between the qubit and the applied microwave field, shows linear dependence on the applied microwave field B_1, Figure 8b,c. Detected linear Rabi oscillations for other samples are shown in Figures S9−S11 given in the SI.

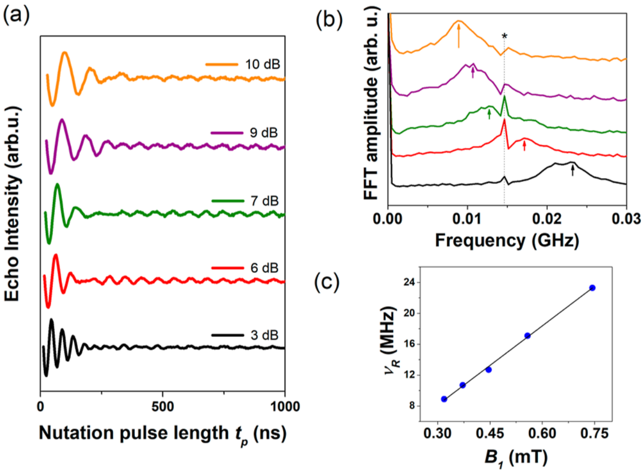

Figure 8. (a) Rabi oscillations recorded for $C_{60}@(VO)_{0.05}$-PCN-223 at 78 K applying different microwave power attenuation. (b) Fast Fourier transform (FFT) of the Rabi oscillations. An asterisk labels the Larmor frequency of proton spins ≈14.5 MHz while arrows label Rabi frequencies. (c) Linear dependence of the Rabi frequency, ν_R, vs the oscillating microwave field, B_1, calculated according to refs 46 and 47.

The Comparison of Vanadyl- and Copper-TCPP Qubits Embedded in PCN-223

The comparison of both relaxation times T_1 and T_m for 10% vanadyl- and 10% copper-TCPP qubits hosted in a PCN-223 matrix can be seen in Figure 9. Copper qubits have longer T_1 below 30 K, as well as T_m below 70 K, compared to the values for vanadyl qubits. However, vanadyl qubits perform better at higher temperatures and maintain coherence up to 240 K, still not being T_1-limited, which makes them better candidates for potential spintronic applications.

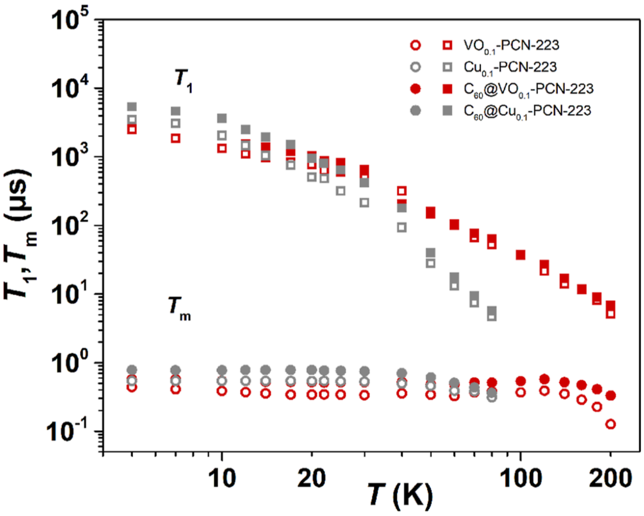

Figure 9. Comparison of temperature dependence of the electron-spin phase-memory relaxation time, T_m, and spin–lattice relaxation time T_1 for 10% copper and 10% vanadyl qubits.

The differences between the studied vanadyl and copper qubits may be due to two main reasons. First, vanadium has one of the smallest spin–orbit couplings among the transition metals.[31,35] This could be best seen from the small difference of vanadium g-values (Table 1) from the free electron values $g = 2.0023$, as this deviation reflects the magnitude of spin–orbit coupling.[31] Larger spin–orbit coupling is associated with reducing T_1 time, resulting in T_m becoming T_1-limited at higher temperatures.[31,67] It is worth noting that the small spin–orbit coupling is the main reason organic radicals and defects exhibit long coherence times.[31] Second, metal–ligand covalency affects the spin–phonon coupling as the non-bonding orbital in vanadyl interacts less strongly with phonons than the antibonding orbital in copper, resulting in longer T_1 time.[31,67,68] Namely, copper(II)-TCPP has more covalent ligand–metal bonds compared to vanadyl-TCPP ions.[31] Vanadyl unpaired spin is located in a nonbonding ionic d_{xy} orbital, while copper spin is in an antibonding $d_{x^2-y^2}$ orbital. This electron spin location is reflected in the previously mentioned observation and nonobservation of superhyperfine interaction with four nitrogen nuclei from the porphyrin core for copper and vanadyl qubits in CW ESR experiments, respectively (Figure 3 in this work, cf. Figure 5 in ref 29). It should be noted, however, that ref 68 reported the opposite effect—for the investigated six-coordinate V(IV) complex, the coherence disappears beyond 100 K, whereas in the four-coordinate Cu(II) dithiocatecholate complexes, the spin echo persists until room temperature, but here, direct comparison is not justified because of different ligand fields around copper(II) and vanadyl centers.[31,68] Overall, the replacement of copper(II) with vanadyl proved particularly beneficial, as the weaker spin–orbit coupling and spin–phonon coupling of the vanadyl center effectively reduce spin–lattice relaxation pathways and quantum decoherence at higher temperatures.

■ CONCLUSIONS

We investigated here the quantum coherence properties of vanadyl-TCPP spin qubits embedded in the moderately porous, 12-coordinated zirconium porphyrinic PCN-223 MOF. Dilution of VO qubits to 10% and 5% with the diamagnetic zinc–TCPP directly influences relaxation processes and extends coherence times. Furthermore, the incorporation of fullerene guests into the MOF pores affected both spin–lattice and phase-memory relaxation times, T_1 and T_m. In addition to the observation of longer relaxation times, we detected prolongation of coherence time for the sample with incorporated fullerene up to 240 K. Notably, at higher dilution, vanadyl centers in PCN-223 yielded exceptionally stable qubits, with phase-memory times extending to $T_m \approx 1$ μs in the nonactivated PCN-223 frameworks. The coherence time is not T_1-limited at 240 K; therefore, there may be room to detect coherence at even higher temperatures. This study demonstrates that the rational design of porphyrin MOFs—through controlled spin dilution and targeted guest inclusion—enables fine-tuning of spin dynamics and environmental interactions. These insights establish that even a moderately porous MOF, such as PCN-223, can serve as a versatile platform for exploring spin coherence in solid-state molecular systems and pave the way for the predictive design of next-generation framework-based quantum devices.

■ ASSOCIATED CONTENT

Supporting Information

The Supporting Information is available free of charge at https://pubs.acs.org/doi/10.1021/acs.inorgchem.5c04870.

Additional FTIR and ESR data and results (PDF)

AUTHOR INFORMATION

Corresponding Authors

Bahar Karadeniz − *Ruđer Bošković Institute, 10000 Zagreb, Croatia*; Email: bahar.karadeniz@irb.hr
Krunoslav Užarević − *Ruđer Bošković Institute, 10000 Zagreb, Croatia*; orcid.org/0000-0002-7513-6485; Email: krunoslav.uzarevic@irb.hr
Dijana Žilić − *Ruđer Bošković Institute, 10000 Zagreb, Croatia*; orcid.org/0000-0003-2387-0853; Email: dijana.zilic@irb.hr

Authors

Lucija Vujević − *Ruđer Bošković Institute, 10000 Zagreb, Croatia*
Gregor Talajić − *Department of Chemistry, University of Zagreb, 10000 Zagreb, Croatia*
Fraser MacMillan − *Institute of Physics, 10000 Zagreb, Croatia*
Alexey A. Popov − *Leibniz IFW Dresden, D-01069 Dresden, Germany*; orcid.org/0000-0002-7596-0378
[⊥]**Marina Kveder** − *Ruđer Bošković Institute, 10000 Zagreb, Croatia*

Complete contact information is available at:
https://pubs.acs.org/10.1021/acs.inorgchem.5c04870

Notes

The authors declare no competing financial interest.
[⊥]Prof. Dr. Marina Kveder deceased on November 26, 2023.

ACKNOWLEDGMENTS

This article is dedicated to the memory of our dear colleague Marina Kveder, who started this research with us as an expert in pulse ESR spectroscopy and who was a great colleague and friend. She passed away on November 26, 2023. The work was supported by the Croatian Science Foundation under the project numbers [HrZZ-IP-2022-10-9292] and [HrZZ-IP-2025-02-5083]. We thank D. Freedman and D. Johnson from MIT for the advice on saturation-recovery experiments.

REFERENCES

(1) Atzori, M.; Sessoli, R. The Second Quantum Revolution: Role and Challenges of Molecular Chemistry. *J. Am. Chem. Soc.* **2019**, *141*, 11339−11352.

(2) Ferrando-Soria, J.; Vallejo, J.; Castellano, M.; Martínez-Lillo, J.; Pardo, E.; Cano, J.; Castro, I.; Lloret, F.; Ruiz-García, R.; Julve, M. Molecular magnetism, quo vadis? A historical perspective from a coordination chemist viewpoint. *Coord. Chem. Rev.* **2017**, *339*, 17−103.

(3) Graham, M. J.; Zadrozny, J. M.; Fataftah, M. S.; Freedman, D. E. Forging Solid-State Qubit Design Principles in a Molecular Furnace. *Chem. Mater.* **2017**, *29*, 1885−1897.

(4) Gaita-Ariño, A.; Luis, F.; Hill, S.; Coronado, E. Molecular spins for quantum computation. *Nat. Chem.* **2019**, *11*, 301−309.

(5) Ngo, T. V.; Tsarev, D. V.; Lee, R.-K.; Alodjants, A. P. Bose−Einstein Condensate Soliton Qubit States for Metrological Applications. *Sci. Rep.* **2021**, *11*, 19363.

(6) de Leon, N. P.; Itoh, K. M.; Kim, D.; Mehta, K. K.; Northup, T. E.; Paik, H.; Palmer, B.; Samarth, N.; Sangtawesin, S.; Steuerman, D. W. Materials Challenges and Opportunities for Quantum Computing Hardware. *Science* **2021**, *372*, No. eabb2823.

(7) Suter, D.; Mahesh, T. S. Spins as qubits: Quantum information processing by nuclear magnetic resonance. *J. Chem. Phys.* **2008**, *128*, 052206.

(8) Degen, C. L.; Reinhard, F.; Cappellaro, P. Quantum Sensing. *Rev. Mod. Phys.* **2017**, *89*, 035002.

(9) Flinn, B. T.; Cull, W. J.; Cardillo-Zallo, I.; Kerfoot, J.; Weare, B. L.; Rance, G. A.; Fay, M. W.; Hernandez, F. U.; Lanterna, A. E.; Mather, M. L.; Khlobystov, A. N. Interactions of Nitrogen-Vacancy Centers in Diamond with Electron Beams: Implications for Quantum Sensing and Photoluminescence Stability. *Adv. Opt. Mater.* **2025**, *13*, No. e02552.

(10) Yamabayashi, T.; Atzori, M.; Tesi, L.; Cosquer, G.; Santanni, F.; Boulon, M.-E.; Morra, E.; Benci, S.; Torre, R.; Chiesa, M.; Sorace, L.; Sessoli, R.; Yamashita, M. Scaling Up Electronic Spin Qubits into a Three-Dimensional Metalic−Organic Framework. *J. Am. Chem. Soc.* **2018**, *140*, 12090−12101.

(11) Ardavan, A.; Rival, O.; Morton, J. J. L.; Blundell, S. J.; Tyryshkin, A. M.; Timco, G. A.; Winpenny, R. E. P. Will Spin-Relaxation Times in Molecular Magnets Permit Quantum Information Processing? *Phys. Rev. Lett.* **2007**, *98*, 057201.

(12) Bertaina, S.; Gambarelli, S.; Mitra, T.; Tsukerblat, B.; Müller, A.; Barbara, B. Quantum oscillations in a molecular magnet. *Nature* **2008**, *453*, 203−207.

(13) Martínez-Pérez, M. J.; Cardona-Serra, S.; Schlegel, C.; Moro, F.; Alonso, P. J.; Prima-García, H.; Clemente-Juan, J. M.; Evangelisti, M.; Gaita-Ariño, A.; Sesé, J.; van Slageren, J.; Coronado, E.; Luis, F. Gd-Based Single-Ion Magnets with Tunable Magnetic Anisotropy: Molecular Design of Spin Qubits. *Phys. Rev. Lett.* **2012**, *108*, 247213.

(14) Wedge, C. J.; Timco, G. A.; Spielberg, E. T.; George, R. E.; Tuna, F.; Rigby, S.; McInnes, E. J. L.; Winpenny, R. E. P.; Blundell, S. J.; Ardavan, A. Chemical Engineering of Molecular Qubits. *Phys. Rev. Lett.* **2012**, *108*, 107204.

(15) Zadrozny, J. M.; Niklas, J.; Poluektov, O. G.; Freedman, D. F. Millisecond coherence time in a tunable molecular electronic spin qubit. *ACS Cent. Sci.* **2015**, *1*, 488−492.

(16) Atzori, M.; Tesi, L.; Morra, E.; Chiesa, M.; Sorace, L.; Sessoli, R. Room-Temperature Quantum Coherence and Rabi Oscillations in Vanadyl Phthalocyanine: Toward Multifunctional Molecular Spin Qubits. *J. Am. Chem. Soc.* **2016**, *138*, 2154−2157.

(17) Jenkins, M. D.; Duan, Y.; Diosdado, B.; García-Ripoll, J. J.; Gaita-Ariño, A.; Giménez-Saiz, C.; Alonso, P. J.; Coronado, E.; Luis, F. Coherent manipulation of three-qubit states in a molecular single-ion magnet. *Phys. Rev. B* **2017**, *95*, 064423.

(18) Godfrin, C.; Ferhat, A.; Ballou, R.; Klyatskaya, S.; Ruben, M.; Wernsdorfer, W.; Balestro, F. Operating Quantum States in Single Magnetic Molecules: Implementation of Grover's Quantum Algorithm. *Phys. Rev. Lett.* **2017**, *119*, 187702.

(19) Wang, C.; Liu, D.; Lin, W. Metal−Organic Frameworks as A Tunable Platform for Designing Functional Molecular Materials. *J. Am. Chem. Soc.* **2013**, *135*, 13222−13234.

(20) Huang, Z.; Geilhufe, R. M. Quantum Metal-Organic Frameworks. *Small Sci.* **2024**, *4*, 2400161.

(21) Yamauchi, A.; Fujiwara, S.; Kimizuka, N.; Asada, M.; Fujiwara, M.; Nakamura, T.; Pirillo, J.; Hijikata, Y.; Yanai, N. Modulation of triplet quantum coherence by guest-induced structural changes in a flexible metal-organic framework. *Nature Commun.* **2024**, *15*, 7622−7629.

(22) Urtizberea, A.; Natividad, E.; Alonso, P. J.; Andrés, M. A.; Gascón, I.; Goldmann, M.; Roubeau, O. A Porphyrin Spin Qubit and Its 2D Framework Nanosheets. *Adv. Funct. Mater.* **2018**, *28*, 1801695.

(23) Zadrozny, J. M.; Gallagher, A. T.; Harris, T. D.; Freedman, D. F. A porous array of clock qubits. *J. Am. Chem. Soc.* **2017**, *139*, 7089−7094.

(24) Yu, C.-J.; Krzyaniak, M. D.; Fataftah, M. S.; Wasielewski, M. R.; Freedman, D. E. A concentrated array of copper porphyrin candidate qubits. *Chem. Sci.* **2019**, *10*, 1702−1708.

(25) Feng, D.; Gu, Z.-Y.; Chen, Y.-P.; Park, J.; Wei, Z.; Sun, Y.; Bosch, M.; Yuan, S.; Zhou, H.-C. A Highly Stable Porphyrinic Zirconium Metal−Organic Framework with shp-a Topology. *J. Am. Chem. Soc.* **2014**, *136*, 17714−17717.

(26) Feng, D.; Chung, W.-C.; Wei, Z.; Gu, Z.-Y.; Jiang, H.-L.; Chen, Y.-P.; Darensbourg, D. J.; Zhou, H.-C. Construction of Ultrastable

Porphyrin Zr Metal−Organic Frameworks through Linker Elimination. *J. Am. Chem. Soc.* **2013**, *135*, 17105−17110.

(27) Hemmer, K.; Boström, H. L.; Krause, S.; Lotsch, B. V.; Fischer, R. A. Strategies to achieve reproducible synthesis of phase-pure Zr-porphyrin metal-organic frameworks. *Commun. Mater.* **2024**, *5*, 264−269.

(28) Karadeniz, B.; Žilić, D.; Huskić, I.; Germann, L. S.; Fidelli, A. M.; Muratović, S.; Lončarić, I.; Etter, M.; Dinnebier, R. E.; Barišić, D.; Cindro, N.; Islamoglu, T.; Farha, O. K.; Friščić, T.; Užarević, K. Controlling the Polymorphism and Topology Transformation in Porphyrinic Zirconium Metal−Organic Frameworks via Mechanochemistry. *J. Am. Chem. Soc.* **2019**, *141*, 19214−19220.

(29) Vujević, L.; Karadeniz, B.; Cindro, N.; Krajnc, A.; Mali, G.; Mazaj, M.; Avdoshenko, S. M.; Popov, A. A.; Žilić, D.; Užarević, K.; Kveder, M. Improving the molecular spin qubit performance in zirconium MOF composites by mechanochemical dilution and fullerene encapsulation. *Chem. Sci.* **2023**, *14*, 9389−9399.

(30) Garlatti, E.; Albino, A.; Chicco, S.; Nguyen, V. H. A.; Santanni, F.; Paolasini, L.; Mazzoli, C.; Caciuffo, R.; Totti, F.; Santini, P.; Sessoli, R.; Lunghi, A.; Carretta, S. The critical role of ultra-low-energy vibrations in the relaxation dynamics of molecular qubits. *Nature Commun.* **2023**, *14*, 1653.

(31) Follmer, A. H.; Ribson, R. D.; Oyala, P. H.; Chen, G. Y.; Hadt, R. G. Understanding Covalent versus Spin−Orbit Coupling Contributions to Temperature-Dependent Electron Spin Relaxation in Cupric and Vanadyl Phthalocyanines. *J. Phys. Chem. A* **2020**, *124*, 9252−9260.

(32) Atzori, M.; Morra, E.; Tesi, L.; Albino, A.; Chiesa, M.; Sorace, L.; Sessoli, R. Quantum Coherence Times Enhancement in Vanadium(IV)-based Potential Molecular Qubits: the Key Role of the Vanadyl Moiety. *J. Am. Chem. Soc.* **2016**, *138*, 11234−11244.

(33) Tesi, L.; Lucaccini, E.; Cimatti, I.; Perfetti, M.; Mannini, M.; Atzori, M.; Morra, E.; Chiesa, M.; Caneschi, A.; Sorace, L.; Sessoli, R. Quantum coherence in a processable vanadyl complex: new tools for the search of molecular spin qubits. *Chem. Sci.* **2016**, *7*, 2074−2083.

(34) Tesi, L.; Lunghi, A.; Atzori, M.; Lucaccini, E.; Sorace, L.; Totti, F.; Sessoli, R. Giant spin−phonon bottleneck effects in evaporable vanadyl-based molecules with long spin coherence. *Dalton Trans.* **2016**, *45*, 16635−16643.

(35) Bader, K.; Winkler, M.; van Slageren, J. Tuning of molecular qubits: very long coherence and spin−lattice relaxation times. *Chem. Commun.* **2016**, *52*, 3623−3626.

(36) Graham, M. J.; Yu, C.-J.; Krzyaniak, M. D.; Wasielewski, M. R.; Freedman, D. E. Synthetic Approach To Determine the Effect of Nuclear Spin Distance on Electronic Spin Decoherence. *J. Am. Chem. Soc.* **2017**, *139*, 3196−3201.

(37) Imperato, M.; Nicolini, A.; Boniburini, M.; Sartini, D.; Benassi, E.; Chiesa, M.; Gigli, L.; Liao, Y.-K.; Raza, A.; Salvadori, E.; Sorace, L.; Cornia, A. Dual Structure of a Vanadyl-Based Molecular Qubit Containing a Bis(β-diketonato) Ligand. *Inorg. Chem.* **2024**, *63*, 7912−7925.

(38) Moisanu, C. M.; Eckvahl, H. J.; Stern, C. L.; Wasielewski, M. R.; Dichtel, W. R. A Paired-Ion Framework Composed of Vanadyl Porphyrin Molecular Qubits Extends Spin Coherence Times. *J. Am. Chem. Soc.* **2024**, *146*, 28088−28094.

(39) Gimeno, I.; Luis, F.; Marcuello, C.; Pallarés, M. C.; Lostao, A.; de Ory, M. C.; Gomez, A.; Granados, D.; Tejedor, I.; Natividad, E.; Urtizberea, A.; Roubeau, O. Localized Nanoscale Formation of Vanadyl Porphyrin 2D MOF Nanosheets and Their Optimal Coupling to Lumped Element Superconducting Resonators. *J. Phys. Chem. C* **2025**, *129*, 973−982.

(40) Puchberger, M.; Kogler, F. R.; Jupa, M.; Gross, S.; Fric, H.; Kickelbick, G.; Schubert, U. Can the Clusters ($Zr_6O_4(OH)_4(OOCR)_{12}$) and ($Zr_6O_4(OH)_4(OOCR)_{12})_2$) Be Converted into Each Other? *Eur. J. Inorg. Chem.* **2006**, *2006*, 3283−3293.

(41) Kickelbick, G.; Schubert, U. Oxozirconium Methacrylate Clusters: $[Zr_6(OH)_4O_4(OMc)_{12})]$ and $[Zr_4O_2(OMc)_{12}]$ (OMc = Methacrylate). *Chem. Ber.* **1997**, *130*, 473−478.

(42) Lu, K.; He, C.; Guo, N.; Chan, C.; Ni, K.; Weichselbaum, R. R.; Lin, W. Chlorin-Based Nanoscale Metal−Organic Framework Systemically Rejects Colorectal Cancers via Synergistic Photodynamic Therapy and Checkpoint Blockade Immunotherapy. *J. Am. Chem. Soc.* **2016**, *138*, 12502−12510.

(43) Schweiger, A.; Jeschke, G. *Principles of Pulse Electron Paramagnetic Resonance*; Oxford University Press: Oxford, 2001.

(44) Eaton, S. S.; Eaton, G. R. Relaxation Times of Organic Radicals and Transition Metal Ions. In: Berliner, L. J., Eaton, G. R., Eaton, S. S., Eds. *Distance Measurements in Biological Systems by EPR. Biological Magnetic Resonance*, vol *19*; Springer, Boston, MA, 2002.

(45) Wolfram Research Inc.. *Mathematica*. version 10, 2024.

(46) Eaton, G. R.; Eaton, S. S.; Quine, R. W.; Mitchell, D.; Kathirvelu, V.; Weber, R. T. A signal-to-noise standard for pulsed EPR. *J. Magn. Reson.* **2010**, *205*, 109−113.

(47) Jeschke, G. *ESR Spectroscopy in Membrane Biophysics*; Springer US: Boston, MA, 2007; pp 17−47.

(48) Martinez, V.; Karadeniz, B.; Biliškov, N.; Lončarić, I.; Muratović, S.; Žilić, D.; Avdoshenko, S. A.; Roslova, M.; Popov, A. A.; Užarević, K. Tunable Fulleretic Sodalite MOFs: Highly Efficient and Controllable Entrapment of C_{60} Fullerene via Mechanochemistry. *Chem. Mater.* **2020**, *32*, 10628−10640.

(49) Smith, T. S.; LoBrutto, R.; Pecoraro, V. L. Paramagnetic spectroscopy of vanadyl complexes and its applications to biological systems. *Coord. Chem. Rev.* **2002**, *228*, 1−18.

(50) Stoll, S.; Schweiger, A. EasySpin, a comprehensive software package for spectral simulation and analysis in EPR. *J. Magn. Reson.* **2006**, *178*, 42−55.

(51) Pace, M. D.; Christidis, T. C.; Yin, J. J.; Milliken, J. EPR of a free radical in fullerene, C_{60}: effect of molecular oxygen. *J. Phys. Chem. A* **1992**, *96*, 6855−6858.

(52) Paul, P.; Kim, K.-C.; Sun, D.; Boyd, P. D. W.; Reed, C. A. Artifacts in the Electron Paramagnetic Resonance Spectra of C_{60} Fullerene Ions: Inevitable $C_{120}O$ Impurity. *J. Am. Chem. Soc.* **2002**, *124*, 4394−4401.

(53) Ranieri, D.; Privitera, A.; Santanni, F.; Urbanska, K.; Strachan, G. J.; Twamley, B.; Salvadori, E.; Liao, Y.-K.; Chiesa, M.; Senge, M. O.; Totti, F.; Sorace, L.; Sessoli, R. A Heterometallic Porphyrin Dimer as a Potential Quantum Gate: Magneto-Structural Correlations and Spin Coherence Properties. *Angew. Chem., Int. Ed.* **2023**, *62*, No. e202312936.

(54) Appleton, J. L.; Le Breton, N.; Carvalho, M.-A.; Weiss, J.; Boudalis, A. K.; Gourlaouen, C.; Choua, S.; Ruppert, R. Vanadyl(IV) Porphyrin Dimers with Palladium(II) and Platinum(II) Linkages: Syntheses, Electronic Properties, and Magnetic Interactions between the Two Moieties. *Cryst. Growth Des.* **2023**, *23*, 1689−1696.

(55) Pozo, I.; Huang, Z.; Lombardi, F.; Alexandropoulos, D. I.; Kong, F.; Slota, M.; Tkach, I.; Bennati, M.; Deng, J.-R.; Stawski, W.; Horton, P. N.; Coles, S. J.; Myers, W. K.; Bogani, L.; Anderson, H. L. Enhanced coherence by coupling spins through a delocalized π-system: Vanadyl porphyrin dimers. *Chem* **2024**, *10*, 299−316.

(56) Eaton, S. S.; Yamabayashi, T.; Horii, Y.; Yamashita, M.; Eaton, G. R. Anisotropy of Spin−Lattice Relaxation Time (T1) for Oxo-Vanadium(IV) and Nitrido Chromium(V) Porphyrins. *J. Am. Chem. Soc.* **2025**, *147*, 13815−13823.

(57) Zadrozny, J. M.; Niklas, J.; Poluektov, O. G.; Freedman, D. F. Multiple Quantum Coherences from Hyperfine Transitions in a Vanadium(IV) Complex. *J. Am. Chem. Soc.* **2014**, *136*, 15841−15844.

(58) Gourier, D.; Delpoux, O.; Bonduelle, A.; Binet, L.; Ciofini, I.; Vezin, H. EPR, ENDOR, and HYSCORE Study of the Structure and the Stability of Vanadyl-Porphyrin Complexes Encapsulated in Silica: Potential Paramagnetic Biomarkers for the Origin of Life. *J. Phys. Chem. B* **2010**, *114*, 3714−3725.

(59) Eaton, S. S.; Eaton, G. R. In Electron Paramagnetic Resonance Investigations of Biological Systems by Using Spin Labels, Spin Probes, and Intrinsic Metal Ions, Part A; Qin, P. Z., Warncke, K., Eds.; *Methods in Enzymology*; Academic Press, 2015; Vol. *563*; pp 37−58.

(60) Chen, H.; Maryasov, A. G.; Rogozhnikova, O. Y.; Trukhin, D. V.; Tormyshev, V. M.; Bowman, M. K. Electron spin dynamics and spin−lattice relaxation of trityl radicals in frozen solutions. *Phys. Chem. Chem. Phys.* **2016**, *18*, 24954−24965.

(61) Kazmierczak, N. P.; Oyala, P. H.; Hadt, R. G. Spectroscopic Signatures of Phonon Character in Molecular Electron Spin Relaxation. *ACS Cent. Sci.* **2024**, *10*, 2353−2362.

(62) Ryan, C.; Briganti, V.; Hogan, C.; O'Neill, M.; Lunghi, A. Spin decoherence in molecular crystals: Nuclear vs electronic spin baths. *J. Chem. Phys.* **2025**, *163*, 134104.

(63) Yu, C.-J.; von Kugelgen, S.; Krzyaniak, M. D.; Ji, W.; Dichtel, W. R.; Wasielewski, M. R.; Freedman, D. E. Spin and Phonon Design in Modular Arrays of Molecular Qubits. *Chem. Mater.* **2020**, *32*, 10200−10206.

(64) Ranieri, D.; Santanni, F.; Privitera, A.; Albino, A.; Salvadori, E.; Chiesa, M.; Totti, F.; Sorace, L.; Sessoli, R. An exchange coupled meso−meso linked vanadyl porphyrin dimer for quantum information processing. *Chem. Sci.* **2022**, *14*, 61−69.

(65) Gimeno, I.; Urtizberea, A.; Román-Roche, J.; Zueco, D.; Camón, A.; Alonso, P. J.; Roubeau, O.; Luis, F. Broad-band spectroscopy of a vanadyl porphyrin: a model electronuclear spin qudit. *Chem. Sci.* **2021**, *12*, 5621−5630.

(66) Fang, Y.-H.; Liu, Z.; Wang, Y. X.; Zhou, S.; Jiang, S.-D.; Gao, S. Orientation mapping of Rabi frequencies in a rare-earth molecular qudit. *Inorg. Chem. Front.* **2020**, *7*, 3875−3881.

(67) Mirzoyan, R.; Hadt, R. G. The dynamic ligand field of a molecular qubit: decoherence through spin−phonon coupling. *Phys. Chem. Chem. Phys.* **2020**, *22*, 11249−11265.

(68) Fataftah, M. S.; Krzyaniak, M. D.; Vlaisavljevich, B.; Wasielewski, M. R.; Zadrozny, J. M.; Freedman, D. F. Metal-ligand covalency enables room temperature molecular qubit candidates. *Chem. Sci.* **2019**, *10*, 6707−6714.